

Article

Antiproliferative Activity of an Organometallic Sn(IV) Coordination Compound Based on 1-Methylbenzotriazole against Human Cancer Cell Lines

Christina Stamou ¹, Chrisavgi Gourdoupi ², Pierre Dechambenoit ³, Dionissios Papaioannou ⁴,
Zoi Piperigkou ^{2,*} and Zoi G. Lada ^{1,*}

¹ Laboratory of Inorganic Chemistry, Department of Chemistry, University of Patras, 26504 Patras, Greece; xrstamou@gmail.com

² Biochemistry, Biochemical Analysis & Matrix Pathobiology Research Group, Laboratory of Biochemistry, Department of Chemistry, University of Patras, 26504 Patras, Greece; up1061190@ac.upatras.gr

³ Environment, Health & Safety Department, University Bordeaux, Centre de Recherche Paul Pascal—CNRS, UMR 5031, F-33600 Pessac, France; pierre.dechambenoit@u-bordeaux.fr

⁴ Department of Chemistry, University of Patras, 26504 Patras, Greece; dapapao@upatras.gr

* Correspondence: zoipip@upatras.gr (Z.P.); zoilada@upatras.gr (Z.G.L.)

Abstract: A motivating class of compounds with interest in the research field of biological active metallopharmaceuticals for cancer treatment is based on organometallic complexes of Sn(IV), exhibiting advantages such as improved cellular uptake and body excretion, lower toxicity, and fewer side effects compared to platinum-based drugs. In this study, the mononuclear organotin coordination complex $[(\text{CH}_3)_2\text{SnCl}_2(\text{mebta})_2]$ was synthesized and characterized using vibrational spectroscopy (IR, Raman), ^1H NMR, $^{13}\text{C}\{^1\text{H}\}$ NMR, and X-ray crystallography. Its antiproliferative properties were thoroughly assessed across an aggressive triple-negative human breast cancer cell line. Notably, comparative studies with precursor materials verified that the observed biological activity is intrinsic to the complex itself. This study highlights the compound's ability to induce cell fate by disrupting essential cellular functions, such as proliferation. By exploring the antiproliferative effects of organotin(IV) derivatives, we introduce a novel class of Sn complexes with 1-methylbenzotriazole (mebta), demonstrating significant potential as promising antitumor agents in the field of organotin compounds.

Keywords: organotin(IV) compounds; antiproliferative activity; 1-methylbenzotriazole; spectroscopic characterization; cytotoxicity



Citation: Stamou, C.; Gourdoupi, C.; Dechambenoit, P.; Papaioannou, D.; Piperigkou, Z.; Lada, Z.G.

Antiproliferative Activity of an Organometallic Sn(IV) Coordination Compound Based on 1-Methylbenzotriazole against Human Cancer Cell Lines. *Chemistry* **2024**, *6*, 1189–1200. <https://doi.org/10.3390/chemistry6050068>

Academic Editor: Guoqi Zhang

Received: 24 July 2024

Revised: 28 September 2024

Accepted: 30 September 2024

Published: 1 October 2024



Copyright: © 2024 by the authors. Licensee MDPI, Basel, Switzerland. This article is an open access article distributed under the terms and conditions of the Creative Commons Attribution (CC BY) license (<https://creativecommons.org/licenses/by/4.0/>).

1. Introduction

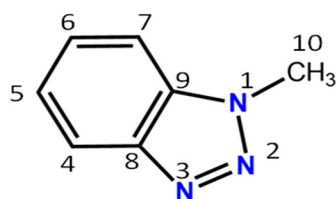
Cytostatic properties are critical in cancer treatment as they inhibit the proliferation of cancer cells, effectively halting tumor growth and preventing metastasis. By leveraging these properties, researchers and clinicians can develop therapies that control cancer progression and enhance patient survival rates [1–3].

The use of platinum-based drugs like cisplatin in cancer treatment spurred intense research into other biologically active non-platinum compounds [4]. Non-platinum metal compounds, such as organotins(IV), are noted for potentially lower toxicity, improved body excretion, and fewer side effects compared to platinum-based drugs [5–10]. A key advantage of organotin(IV) compounds is that they do not induce chemoresistance, possibly offering lower toxicity relative to cisplatin analogs [11–13]. Cancer research towards the anticancer activity of organotin(IV) compounds derived from Marcel Gielen in the 80s [14], being the stepping stone for the numerous studies that followed. Based on these studies, several parameters could affect the efficiency of the metallodrugs, including the coordination sphere of the compound and the type of the organic ligand [15–17]. In particular, based on Structure Activity Relationship (SAR) of organotin(IV) compounds,

it is known nowadays that their biological activity is closely connected to the availability of coordination positions on Sn, the occurrence of relatively stable ligand–Sn bonds, and slow hydrolytic decomposition behavior [18]. In parallel, the R group of the organic ligand may play an important role on the lipophilicity of the drug. The dominant mechanism of organotin compounds is to trigger apoptosis by attaching to the external phosphate groups of DNA and disrupting the intracellular metabolism of phospholipids.

Compounds represented by the formula R_ySnX_{4-y} (where X = Cl or Br) contain an Sn(IV) atom and are categorized as mono-, di-, tri-, or tetraorganotins depending on the number of alkyl or aryl groups attached to the tin atom. Organotin chlorides are known to induce lipid peroxidation in cell membranes, resulting in oxidative stress [19]. These R_ySnX_{4-y} compounds, recognized for their antitumor activity, interact with DNA to impact cell death mechanisms through necrosis, elevate extracellular Ca^{2+} levels, and generate reactive oxygen species (ROS), thereby promoting apoptosis [19].

Developed in the late 1960s, azoles are a prominent class of heterocyclic compounds and represent a prevailing part of antifungal drugs available [20]. Benzotriazoles are important “players” in biomedical research due to a plethora of antimicrobial, antiparasitic, choleric, and cholesterol-lowering properties; in addition, they have been reported as antiproliferative agents [21]. The popularity of benzotriazoles in organic [22] and inorganic [23] chemistry is tremendous. The rationale behind the present work was an effort to combine the antitumor properties of organotins and benzotriazoles. In addition, 1-methylbenzotriazole (mebta, Scheme 1) could be a promising ligand [24] for organotin complexes with potential antitumor properties. Its ability to form stable complexes with organotin may enhance the biological activity and efficacy of these compounds in targeting cancer cells.



Scheme 1. The structural formula of the 1-methylbenzotriazole ligand.

In this study, the mononuclear organotin coordination complex $[(CH_3)_2SnCl_2(mebta)_2]$ was synthesized. This compound has been characterized by different spectroscopic methods including vibrational spectroscopy (IR, Raman), 1H -NMR and $^{13}C\{^1H\}$ -NMR, along with the determination of its crystal structure by X-ray analysis. The cytotoxic activity was accessed in detail on aggressive triple-negative breast cancer cells to evaluate the influence of this compound on cell viability. This study was also performed for the pristine starting materials in order to verify that the biological activity is attributed to the complex and not to the ligand or the initial Sn starting material. The intrinsic ability of a compound to cause cell death by disrupting essential cellular functions, such as cell proliferation, is considered a key cytotoxic property. We do believe that the present effort could initiate a new class of organotin Sn complexes with 1-methylbenzotriazole (mebta), being so far unknown in the literature, with potential interesting biological properties as alternatives of other organotin antiproliferative compounds.

2. Materials and Methods

2.1. Materials and Spectroscopic-Physical Measurements

All synthetic procedures were performed under aerobic conditions. Distilled water was received from the in-house facility. Solvents and reagents were purchased from Sigma-Aldrich (Tanfrichen, Germany) and Alfa Aesar (Karlsruhe, Germany), and used as received without further purification. Dimethyltin dichloride (CAS: 753-73-1) was purchased by Sigma-Aldrich and 1-methylbenzotriazole, abbreviated as mebta (CAS: 13351-73-0),

was purchased by Alfa Aesar with purity > 99.9% and >98%, respectively. The purity of the starting materials and the product was checked by carbon, hydrogen, and nitrogen microanalyses, performed by the Instrumental Analysis Laboratory of the University of Patras. KBr pellets of the complex, the mebta organic ligand, and the organotin reagent were prepared under pressure and the FT-IR spectra were recorded using a Perkin-Elmer spectrometer (16PC, Perkin-Elmer, Waltham, MA, USA). Raman spectra were recorded by a T-64000 Jobin Yvon-Horiba micro-Raman setup operating under a single-spectrograph configuration. The excitation wavelength for mebta was 514.5 nm emitted from a DPSS laser (Cobolt Fandango TMISO Laser, Norfolk, UK). The Raman spectrum of complex 1 was recorded by a 632.8 nm excitation line, emitted from the HeNe laser source (Optronics Technologies S.A., Model HLA-20P, 20 mW, Moschato, Greece); the collection of Raman spectrum was not possible by using the 514.5 nm excitation due to overlapping fluorescence during the measurement. The laser power on the samples was 1 mW. The backscattered radiation was collected from a single configuration of the monochromator after passing through an appropriate edge filter (LP02-633RU-25, Laser2000 Ltd., Huntingdon, Cambridgeshire, UK). The calibration of the instrument was achieved via the standard peak position of Si at 520.5 cm^{-1} . The spectral resolution was 5 cm^{-1} . NMR spectra were recorded using Varian VnmrS 500 (500 MHz for ^1H NMR and 126 MHz for $^{13}\text{C}\{^1\text{H}\}$ NMR). UV/Vis spectra in solution were recorded on a Hitachi U-300 spectrometer. Conductivity measurements were carried out at $25\text{ }^\circ\text{C}$ with a Metrohm-Herisau E-527 bridge; the concentration of complex 1 was ca. 10^{-3} M .

2.2. Preparation of the Complex

$[(\text{CH}_3)_2\text{SnCl}_2(\text{mebta})_2]$ (1): In a solution of 1-methylbenzotriazole (0.027 g, 0.20 mmol) in CH_2Cl_2 (6 mL) was added an amount of solid $(\text{CH}_3)_2\text{SnCl}_2$ (0.022 g, 0.10 mmol). The resulting colorless solution was stirred for 20 min, filtered, and allowed to slowly evaporate at room temperature. X-ray quality, colorless crystals of the product were obtained within 7 d. The crystals were collected by filtration, washed with cold CH_2Cl_2 ($2 \times 0.5\text{ mL}$) and Et_2O ($2 \times 2\text{ mL}$), and dried in vacuo over anhydrous CaCl_2 . Yield: 52%. Anal. Calcd. (%) for $\text{SnCl}_2\text{C}_{16}\text{N}_6\text{H}_{20}$: C, 39.54; H, 4.15; N, 17.3. Found (%): C, 39.21; H, 4.64; N, 17.78. IR (KBr, cm^{-1}): 3093 (w), 3026 (w), 2934 (w), 1946 (w), 1812 (w), 1720 (w), 1590 (w), 1493 (m), 1455 (s), 1309 (m), 1270 (s), 1222 (s), 1171 (m), 1136 (w), 1058 (m), 1001 (w), 935 (m), 861 (w), 764 (s), 736 (m), 659 (w), 588 (m), 529 (m), 499 (m), 437 (m). ^1H NMR (500 MHz, $\text{dms}\text{-d}_6$) δ 8.03 (dt, $J = 8.4, 0.9\text{ Hz}$, 2H), 7.84 (dt, $J = 8.3, 1.0\text{ Hz}$, 2H), 7.58–7.53 (m, 2H), 7.40 (ddd, $J = 8.3, 6.9, 1.0\text{ Hz}$, 2H), 4.31 (s, 6H), 1.03 (s, 6H). $^{13}\text{C}\{^1\text{H}\}$ NMR (126 MHz, $\text{dms}\text{-d}_6$) δ 145.09, 133.33, 127.08, 123.85, 118.97, 110.56, 34.11, 22.69.

2.3. Single-Crystal X-ray Crystallography

The crystallographic data were collected with a Bruker APEX II Quasar diffractometer, equipped with a graphite monochromator centered on the path of Mo $\text{K}\alpha$ radiation. Colorless single crystals were coated with CargilleTM NHV immersion oil and mounted on a fiber loop, followed by data collection at 120 K. The program SAINT was used to integrate the data, which was thereafter corrected using SADABS [25]. The structure was solved using SHELXT [26] and refined by a full-matrix least-squares method on F^2 using SHELXL-2019 [27]. All non-hydrogen atoms were refined with anisotropic displacement parameters, whereas hydrogen atoms were assigned to ideal positions and refined isotropically using a suitable riding model.

The CIF file has been deposited at the Cambridge Crystallographic Data Centre as supplementary publication no. CCDC 2370835.

2.4. Cytostatic Analysis

Biochemicals and reagents

Dulbecco's modified essential medium (DMEM), fetal bovine serum (FBS), sodium pyruvate, L-glutamine, penicillin, streptomycin, amphotericin B, and gentamycin were all

obtained from Biosera LTD (France). All other chemicals used were of the best commercially available grade.

Cell cultures and conditions

MDA-MB-231 triple-negative breast cancer cell line was obtained from the American Type Culture Collection (ATCC, Baltimore, MD, USA) and routinely cultured as monolayers at 37 °C in a humidified atmosphere of 5% (*v/v*) CO₂ and 95% air. Cells were grown in complete DMEM culture medium supplemented with 10% FBS, a cocktail of antimicrobial agents (100 IU/mL penicillin, 100 mg/mL streptomycin, 10 mg/mL gentamicin sulphate and 2.5 mg/mL amphotericin B), 2 mM L-glutamine and 1 mM sodium pyruvate. Cells were harvested by trypsinization with 0.05% (*w/v*) trypsin in PBS containing 0.02% (*w/v*) Na₂EDTA. All experiments were conducted in serum-free conditions (0% FBS), to remove the net effects of serum. The tested compounds were dissolved in 100% DMSO at a 1 mg/mL concentration of each stock solution and the serial dilutions for final concentrations 0.05, 0.5, 1, 5, 10 µg/mL (0.10–20.58 µM), according to each experimental design were performed in DMEM 0% FBS. Concentration range was 0.10–20.58 µM, 0.38–75.1 µM, and 0.23–45.52 µM, for complex 1 (485.93 g/mol), mebta (133.15 g/mol), and (CH₃)₂SnCl₂ (219.68 g/mol), respectively. DMSO concentration range in the working solutions of the tested compounds was 0.05–2.5% *v/v*, accordingly. Cells were treated with the complex and its substitutes for 24 h prior to each experimental procedure. To note, vehicle controls with the respective concentration of DMSO as in the tested compounds have been included in each experimental procedure. The highest DMSO concentration used did not significantly affect cell viability.

Phase contrast microscopy

MDA-MB-231 cells were seeded into 96-well plates at a density of 5000 cells per well. Cells were incubated in complete medium (DMEM, 10% FBS) for 24 h and then the medium was changed to serum-free, and the cells were serum starved overnight prior to treatment with complex 1 (10 µg/mL). For phase-contrast microscopy, images of live cells growing on the culture dish were collected on an OLYMPUS CKX41 microscope equipped with a CMOS color digital camera (SC30).

WST-1 cell viability assay

MDA-MB-231 breast cancer cells were seeded into 96-well plates at a density of 5000 cells per well. Cells were incubated in complete medium (DMEM, 10% FBS) for 24 h and then the medium was changed to serum-free, and the cells were serum starved overnight prior to treatment with the tested compounds for 24 h in the concentration range 0.05–10 µg/mL. Briefly, WST-1 premix reagent was added in each well at 1:10 ratio and the absorbance at 450 nm was measured (reference wavelength at 650 nm), according to the manufacturer's instructions.

Statistical analysis

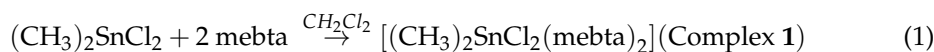
For each assay, three individual experiments were conducted. Data in diagrams are expressed as mean ± standard deviation (SD). Statistical analyses and graphs were made using GraphPad Prism 9 (GraphPad Software, San Diego, CA, USA). Statistically significant differences are indicated by asterisks: * ($p \leq 0.05$), compared with untreated (control) cells. Non-statistically significant comparisons ($p > 0.05$) are not displayed.

3. Results

3.1. Synthetic Comments

Different synthetic attempts were performed for the investigation of the (CH₃)₂SnCl₂/mebta system. The solvent that gave the best crystals was CH₂Cl₂. It is interesting that complex 1 was isolated by using another solvent (i.e., MeOH) apart from CH₂Cl₂ (microanalytical and IR evidence), but not with MeCN. In addition, both a 1:1 and 1:2 ratio between (CH₃)₂SnCl₂ and mebta resulted in the precipitation of the product. This is encouraging since from a synthetic point of view, it implies a rather stable product that could

be easily obtained by different synthetic conditions. The colorless crystals of complex **1** suitable for single-crystal X-ray analysis were obtained from closed vials after a week; the stoichiometric equation is presented in Equation (1).



3.2. Characterization of the Products

3.2.1. Vibrational Spectroscopy

The IR spectrum of (**1**) is presented in Figure S1, along with the IR spectrum of the organic ligand (mebta). In the IR spectrum of mebta, the stretching vibrations attributed to the aromatic ($3000\text{--}3100 \text{ cm}^{-1}$) and the aliphatic ($2900\text{--}3000 \text{ cm}^{-1}$) C-H group are present. In the spectral region $1650\text{--}1500 \text{ cm}^{-1}$, the C=C and C=N bond stretching was observed at 1647 and 1590 cm^{-1} . The C-H deformations and the C-N stretching appear in the region $1450\text{--}1300 \text{ cm}^{-1}$, while the aromatic C-H in-plane and out-of-plane deformations are shown in the spectral region $1250\text{--}1000 \text{ cm}^{-1}$ and $1000\text{--}700 \text{ cm}^{-1}$, respectively. The vibration at around 650 cm^{-1} is attributed to the C=N and N=N bonds. The majority of these peaks that are involved in the coordination, especially the vibrations of the C=N, C-N bonds, are shifted upwards in complex **1** suggesting coordination of the ring-N atom to Sn(IV) [28].

In parallel, the Raman spectra of complex **1** and mebta were recorded (Figure 1). Apparently, as in the IR spectrum, the characteristic vibrations of mebta are also present. In addition, the presence of the $(\text{CH}_3)_2\text{SnCl}_2$ unit is also evident in the spectrum. In particular, the stretching vibrations noticed at 342 and 553 cm^{-1} are attributed to the Sn-Cl asymmetric and the Sn-C symmetric vibrations, respectively [29]. It is important to note that the excitation laser line used for the measurement did not promote any Resonance Raman effects, since based on the UV/Vis spectrum of the complex, there is no evidence of an absorption band in the wavelength range $500\text{--}800 \text{ nm}$.

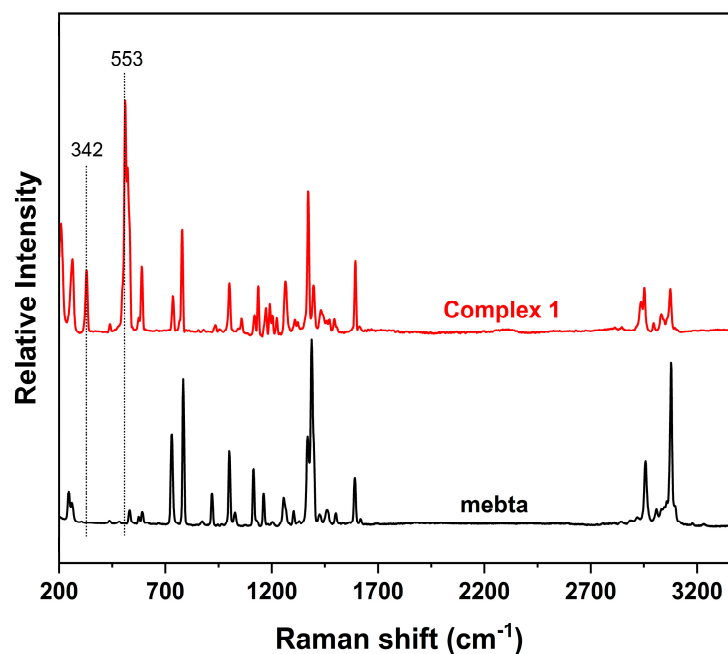


Figure 1. The Raman spectrum of complex $[(\text{CH}_3)_2\text{SnCl}_2(\text{mebta})_2]$ (**1**) is presented with red and the Raman spectrum of 1-methylbenzotriazole (mebta) is presented in black.

3.2.2. ^1H and $^{13}\text{C}\{^1\text{H}\}$ NMR Spectroscopy

The ^1H NMR and $^{13}\text{C}\{^1\text{H}\}$ NMR spectra were recorded in d_6 -DMSO solutions for complex **1** in order to investigate the purity of the complex and the stability of the sample in d_6 -DMSO, which is the medium that was used for the subsequent cytostatic measurements.

In Figure 2a the ^1H NMR spectrum of complex **1** (Figure 2a) is presented. It is evident that the ^1H NMR spectrum shows all the characteristic signals attributed to the ligand mebta in the aromatic area (i.e., δ 8.03 (dt, $J = 8.4, 0.9$ Hz, 2H), 7.84 (dt, $J = 8.3, 1.0$ Hz, 2H), 7.58–7.53 (ddd, $J = 8.4, 6.9$ and 0.9 Hz, 2H), 7.40 (ddd, $J = 8.3, 6.9, 1.0$ Hz, 2H)), and the signal at δ 4.31 (s, 6H) in the aliphatic region, which is in accordance with previous experimental and theoretical analysis of mebta [28,30]. In addition to these signals, the signal in the aliphatic region (i.e., δ 1.03 ppm) is due to the co-existence of the two CH_3 groups of the $(\text{CH}_3)_2\text{SnCl}_2$ in the product. This is also supported by the HSQC NMR spectrum of the complex (Figure S2) where the satellite peaks are clearly observed. The $^2J(^1\text{H}, ^{117}\text{Sn})$ and $^2J(^1\text{H}, ^{119}\text{Sn})$ coupling constants were calculated to be 109 and 113.67 Hz, respectively (Figure S3), which is in close proximity to analogous coordination complexes [31,32].

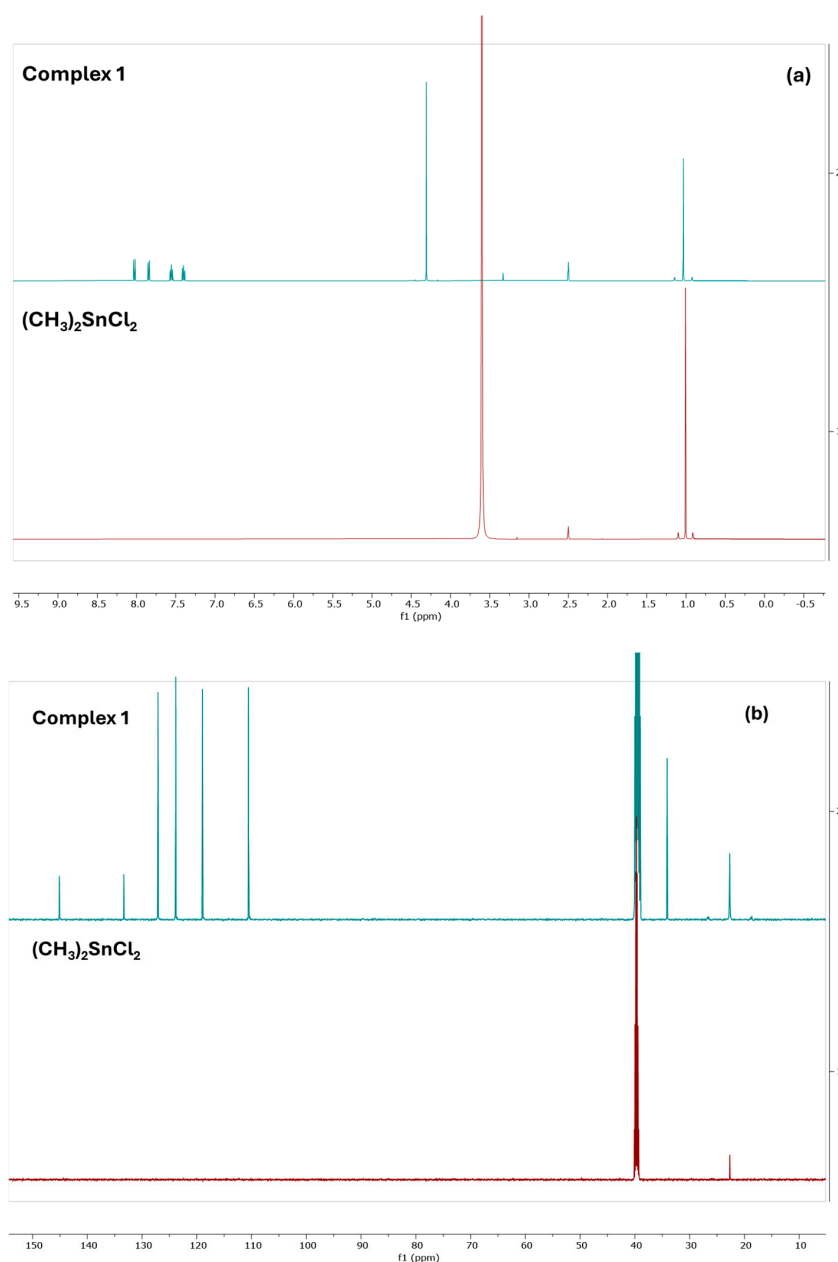


Figure 2. (a) The ^1H NMR spectra of complex $[(\text{CH}_3)_2\text{SnCl}_2(\text{mebta})_2]$ (**1**) and $(\text{CH}_3)_2\text{SnCl}_2$ in d_6 -DMSO. (b) The $^{13}\text{C}\{^1\text{H}\}$ NMR spectra of **1** and $(\text{CH}_3)_2\text{SnCl}_2$ in d_6 -DMSO. The signals at δ 2.52 ppm and \sim 3.6 ppm in the ^1H NMR spectra are due to the protons of the non-deuterated solvent and to the protons of the H_2O contained in d_6 -DMSO, respectively. The signal at $\delta \sim 40$ ppm in the $^{13}\text{C}\{^1\text{H}\}$ NMR spectra is due to the carbon atoms of the solvent.

In a similar way, in the $^{13}\text{C}\{^1\text{H}\}$ NMR spectrum of complex **1** (Figure 2b), all the characteristic signals of mebta attributed to the aromatic carbons are shown in the range 110–150 ppm (i.e., δ 145.09, 133.33, 127.08, 123.85, 118.97, 110.56 ppm) further supported by the previous $^{13}\text{C}\{^1\text{H}\}$ NMR analysis of the ligand [28,30]. The signal at δ 34.11 ppm in the spectrum of **1** is assigned to the carbon atoms of the CH_3 groups of both mebta ligands whereas the carbon atoms of the coordinated methyl groups resonate at δ 22.69 ppm. The latter appears at δ 22.49 ppm in the spectrum of $(\text{CH}_3)_2\text{SnCl}_2$. The assignment of these two kinds of carbon atoms is supported by the HSQC spectrum of complex **1** (Figure S2) where they show cross-peaks with their corresponding protons resonating at δ 4.31 and 1.03 ppm, respectively. The ^1H NMR and $^{13}\text{C}\{^1\text{H}\}$ NMR δ values of mebta in **1** are slightly different than the corresponding ones in the free ligand, implying that mebta remains coordinated in solution. The stability of the complex in DMSO is further proven by its molar conductivity in the same solvent, Λ_{M} (10^{-3} M, 25 °C, DMSO), which is $3 \text{ S cm}^2 \text{ mol}^{-1}$; this value is indicative of the presence of neutral species in solution [33] suggesting no decomposition through Cl^- release. The above experimental facts strongly suggest that the solid-state structure is retained in solution. In addition, the stability of the complex after 24 h was confirmed by ^1H NMR measurements with time ($t = 0, 0.5 \text{ h}, 1 \text{ h}, 4 \text{ h}$ and 24 h) (Figure S4) [34]. This stability is crucial for the biological study, thus the stock solutions have been prepared in DMSO, which were then diluted in serum-free cell culture medium for each experimental procedure. In this context, future work will include stability studies of the Sn(IV) complex in aqueous media, particularly the hydrolysis rates of chloride ligands.

3.2.3. UV/Vis Spectroscopy

The UV/Vis spectrum of the complex **1** (Figure 3) was recorded in a solution of 82 μM in methanol (MeOH), showing the characteristic $\pi\text{-}\pi^*$ transitions of the organic ligand. The absence of absorbance peaks at the range 400–700 nm ensures that there is no interference of Resonance Raman effects during the Raman measurements.

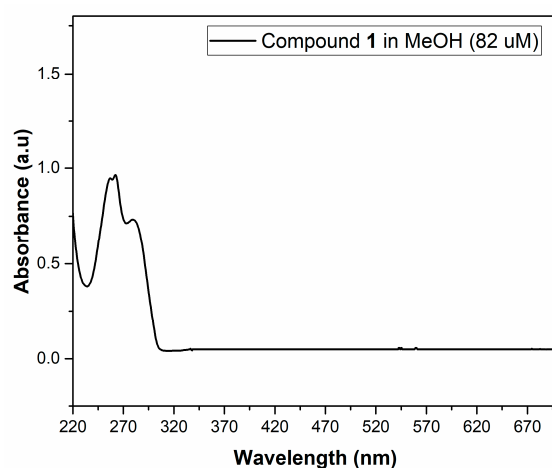


Figure 3. The UV/Vis spectrum of complex $[(\text{CH}_3)_2\text{SnCl}_2(\text{mebta})_2]$ (**1**) in MeOH ($c = 82 \mu\text{M}$).

3.3. Description of the Molecular Structure and Packing

Structural illustration of the molecule $[(\text{CH}_3)_2\text{SnCl}_2(\text{mebta})_2]$ (**1**) is provided in Figure 4. Complex **1** crystallizes in the triclinic space group P-1 (no 2). The Sn^{IV} center is located at a crystallographically imposed inversion center. The metal ion is coordinated to 2 terminal monodentate mebta ligands through one N atom of the triazole ring; this atom is the nitrogen of the position 3 of theazole ring, see Scheme 1. The octahedral coordination sphere of Sn^{IV} (coordination number = 6) is completed by two Cl^- and two CH_3^- ligands. Typical bond lengths for an octahedral organotin(IV) complex were observed [35,36]. Selected interatomic distances (\AA) and angles ($^\circ$) are provided in the Figure 4 caption, indicating the octahedral configuration of the complex. The main crystallographic data of complex

1 ($C_{16}H_{20}Cl_2N_6Sn$) could be summarized as follows: triclinic, P-1 (no. 2), $a = 7.1665(4)$, $b = 7.7958(4)$, $c = 9.5437(5)$ Å, $\alpha = 111.720(2)^\circ$, $\beta = 110.205(2)^\circ$, $\gamma = 90.404(2)^\circ$, $V = 459.26(4)$ Å³, $Z = 1$, $T = 120$ K, 11,307 reflections measured, 2479 unique ($R_{int} = 0.0184$), $\theta_{max} = 29.211^\circ$ $GoF = 1.126$, $R_1 = 0.0118$, wR_2 (all reflections) = 0.0328.

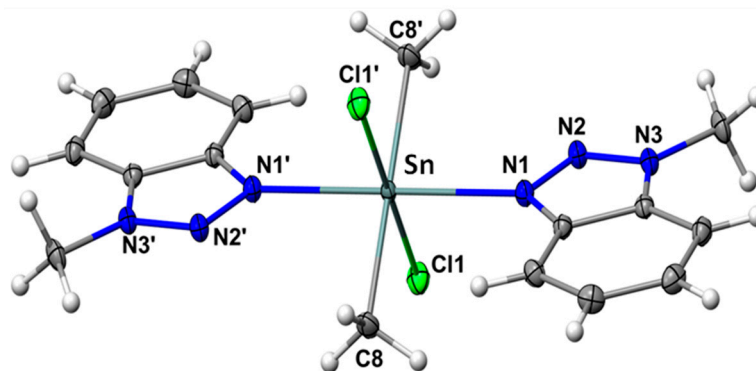


Figure 4. ORTEP-type view of complex **1** in the crystal at 120 K. The thermal ellipsoids are depicted for the non-H atoms at a 50% probability level. C: grey, H: white, N: blue, O: red, Cl: light green, Sn: cyan. Selected interatomic distances (Å) and angles ($^\circ$): $N1 - Sn = 2.376$, $C8 - Sn = 2.113$, $Cl1 - Sn = 2.575$ and $N1 - Sn - N1' = Cl1 - Sn - Cl1' = C8 - Sn - C8' = 180.0$. Primed atoms have been generated by the symmetry operation $-x + 1, -y + 1, -z$.

In the crystal, the aromatic rings of the complex molecules are π -stacked to form a 2D supramolecular network by π - π interactions along the (ac) plane (Figure 5). The distance between the planes formed by the aromatic rings is ca. 3.47 Å. These 2D networks pack along the third dimension of the crystal without specific directional interactions (Figure S5).

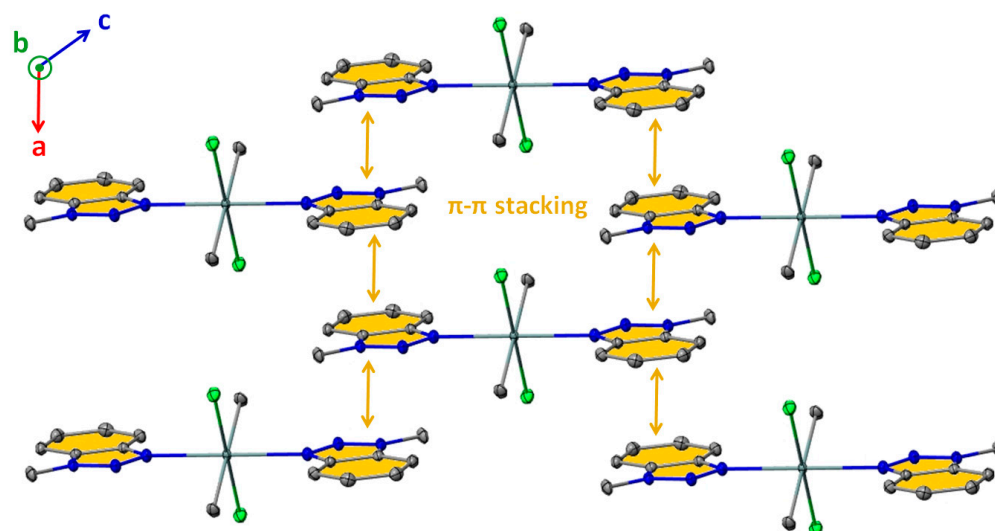


Figure 5. Packing of the complexes along the (ac) plane, forming a 2D supramolecular network by π - π interactions. The distance between the planes formed by the aromatic rings is ca. 3.47 Å. The thermal ellipsoids are depicted for the non-H atoms at the 50% probability level. C: grey, H: white, N: blue, O: red, Cl: light green, Sn: cyan.

3.4. Investigation of Antiproliferative Properties

We evaluated the potential antiproliferative effects of complex **1** and its “components” in terms of the cell viability of triple-negative breast cancer cells, MDA-MB-231. MDA-MB-231 cells were treated for 24 h in the concentration range 0.05–100 $\mu\text{g}/\text{mL}$ at 10 $\mu\text{g}/\text{mL}$ increment (selective concentrations are shown in Figure 6), in order to define the effective antiproliferative concentration of complex **1** and the effects, if any, of its “components”. As

shown in Figure 6, no significant cytotoxicity is observed at concentrations 0.05–10 $\mu\text{g}/\text{mL}$ for complex 1, while at the highest concentration, 10 $\mu\text{g}/\text{mL}$, complex 1 statistically significantly reduces MDA-MB-231 cell viability at 75% ($\text{IC}_{50} \sim 20 \mu\text{M}$). Notably, we observed no significant effects on cell viability of MDA-MB-231 cells treated for 24 h with either mebta or $(\text{CH}_3)_2\text{SnCl}_2$ (Figure 6b,c). Moreover, as shown in Figure 6d, we evaluated the effects of complex 1 in the most effective concentration (10 $\mu\text{g}/\text{mL}$) in terms of cell morphology. MDA-MB-231 breast cancer cells typically appear elongated and spindle-like in the traditional 2D monolayers. As depicted in Figure 6d, no significant effects on MDA-MB-231 cell morphology were observed; however, the formation of cell aggregates and junctions may be linked to the reduced cell viability in the presence of complex 1.

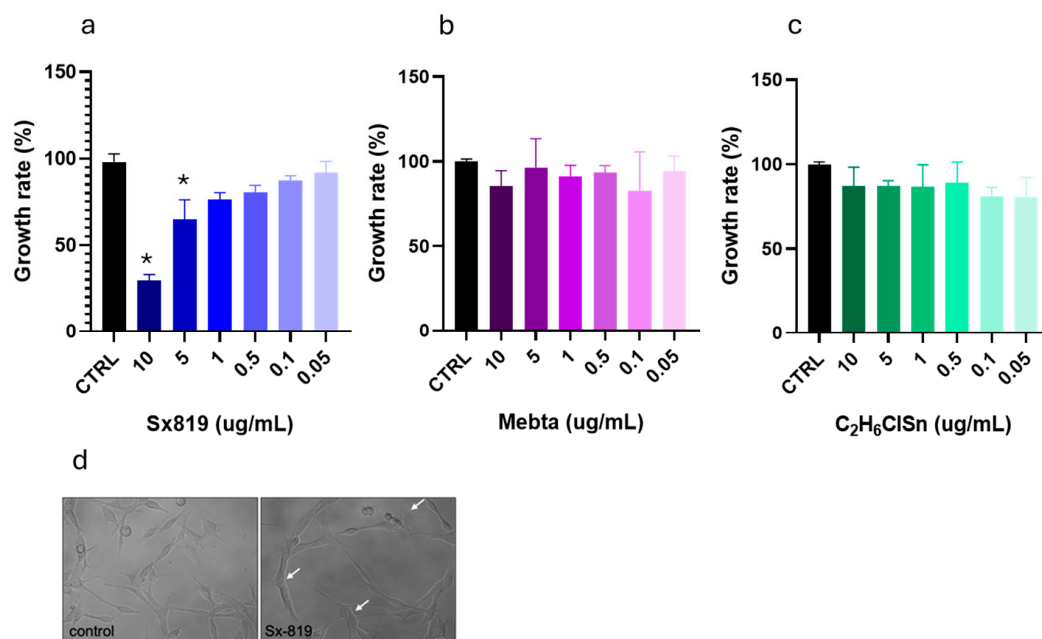


Figure 6. Effects of complex 1 on cell viability and morphology of MDA-MB-231 breast cancer cells: (a) WST-1 cell viability following 24 h treatment of MDA-MB-231 cells with concentrations of 0.05, 0.1, 0.5, 1, 5, 10 $\mu\text{g}/\text{mL}$ (0.10–20.58 μM) of complex 1 for 24 h; (b) WST-1 cell viability following treatment of mebta in the same concentrations (0.38–75.1 μM) with complex 1 for 24 h; (c) WST-1 cell viability following treatment of $(\text{CH}_3)_2\text{SnCl}_2$ in the same concentrations (0.23–45.52 μM) with complex 1 for 24 h; (d) phase-contrast microscopy to monitor cellular morphology of MDA-MB-231 cells before (control) and after complex 1 treatment (20.58 μM). Cell junctions are shown with arrows (magnification 40 \times). The asterisk (*) indicates statistically significant difference ($p \leq 0.05$).

Collectively, we have highlighted the promising role of the organotin(IV) complex 1 in reducing the proliferative rates of the aggressive triple-negative breast cancer cells and that this effect is due to the whole complex and not to its ingredients, i.e., mebta and/or $(\text{CH}_3)_2\text{SnCl}_2$.

4. Conclusions

A new organotin coordination complex, i.e., $[(\text{CH}_3)_2\text{SnCl}_2(\text{mebta})_2]$, was synthesized. In the crystal structure of the complex, π - π interactions result in a 2D supramolecular network. The vibration spectroscopy (IR and Raman) verified the successful synthesis and the purity of the complex. No resonance effects intervene to the Raman spectra as it was verified through UV/Vis spectroscopy. In addition, NMR study (^1H NMR and $^{13}\text{C}\{^1\text{H}\}$ NMR) revealed the stability of the complex in DMSO, which was the solvent used for the cytotoxicity measurements. Complex 1 reduces the proliferative rates of the aggressive triple-negative breast cancer cells with a significantly reduction of MDA-MB-231 cell viability at 75% ($\text{IC}_{50} \sim 20 \mu\text{M}$), while this effect was not observed for the two

starting materials used for the preparation of complex **1**. The present study introduces the potential of the development of a new class of mixed organometallic-coordination Sn(IV) compounds with benzotriazole ligation, with preferential profile as antiproliferative agents in aggressive breast cancer cells. In future, studies investigating the biological effects of these promising compounds as cytotoxic complexes for breast cancer cells, the use of cytostatic agents, such as cytarabine, as controls in functional assays (i.e., cell mobility studies) or incorporating cell cycle assessments, may effectively address and evaluate the compounds' cytostatic impact. The interplay between estrogen receptor signaling and intercellular matrix components is a key factor in understanding the regulatory mechanism on breast cancer cell functional properties [37]. Work in progress in our laboratories is directed towards the study of the effect of the nature of the organometallic ligand R, the halide ligand, and the benzotriazole group in complexes $[R_2SnX_2L_2]$, where R = Et, Ph, X = Br, I and L = various neutral benzotriazole ligands, and the development of SAR criteria. We have been also working in the preparation and study of the antiproliferative properties in compounds of the general type $[R_3SnXL_2]$.

Supplementary Materials: The following supporting information can be downloaded at: <https://www.mdpi.com/article/10.3390/chemistry6050068/s1>. Figure S1. The FT-IR spectrum of complex $[(CH_3)_2SnCl_2(mebta)_2]$ (**1**) presented in purple and the FT-IR spectrum of 1-methylbenzotriazole presented in red. Figure S2. The HSQC spectrum of complex **1** in the aliphatic region. Figure S3. Calculation of the $^{117/119}Sn-^1H$ couplings with the aid of the satellites of the Sn-CH₃ group. Figure S4. The 1H NMR spectra of complex $[(CH_3)_2SnCl_2(mebta)_2]$ (**1**) at different incubation times (t = 0, 0.5 h, 1 h, 4 h, and 24 h). Within the red square the region 7.3 to 8.5 has been zoomed in. Figure S5. Projection of the crystal structure along the (bc) plane, showing the packing of the 2D supramolecular network along the (ac) plane. The thermal ellipsoids are depicted for the non-H atoms at the 50% probability level. C: grey, H: white, N: blue, O: red, Cl: light green, Sn: cyan.

Author Contributions: Z.G.L.: investigation, methodology, writing—review and editing, supervision, project administration, resources, data curation; C.S.: methodology, investigation, data curation; C.G.: methodology, investigation; P.D.: methodology, investigation, data curation, writing—review and editing; D.P.: data curation, review and editing; Z.P.: supervision, writing—review and editing, resources, data curation. All authors have read and agreed to the published version of the manuscript.

Funding: Z.P. acknowledges the funding program “MEDICUS” of the University of Patras, Greece. Grant Number: 82718.

Data Availability Statement: The data that support the findings of this study are available from the corresponding author upon reasonable request.

Conflicts of Interest: The authors declare no conflict of interest.

References

1. Ioele, G.; Chieffallo, M.; Occhiuzzi, M.A.; De Luca, M.; Garofalo, A.; Ragno, G.; Grande, F. Anticancer Drugs: Recent Strategies to Improve Stability Profile, Pharmacokinetic and Pharmacodynamic Properties. *Molecules* **2022**, *27*, 5436. [CrossRef] [PubMed]
2. Anttila, J.V.; Shubin, M.; Cairns, J.; Borse, F.; Guo, Q.; Mononen, T.; Vázquez-García, I.; Pulkkinen, O.; Mustonen, V. Contrasting the impact of cytotoxic and cytostatic drug therapies on tumour progression. *PLoS Comput. Biol.* **2019**, *15*, e1007493. [CrossRef] [PubMed]
3. Grijalva, M.; Vallejo-López, M.J.; Salazar, L.; Camacho, J.; Kumar, B. Cytotoxic and antiproliferative effects of nanomaterials on cancer cell lines: A review. In *Unraveling the Safety Profile of Nanoscale Particles and Materials—From Biomedical to Environmental Applications*; InTech: Takasago, Japan, 2018; pp. 63–85.
4. Kaluderovic, G.; Paschke, R. Anticancer Metallotherapeutics in Preclinical Development. *Curr. Med. Chem.* **2011**, *18*, 4738–4752. [CrossRef] [PubMed]
5. Hadjikakou, S.K.; Hadjiliadis, N. Antiproliferative and anti-tumor activity of organotin compounds. *Coord. Chem. Rev.* **2009**, *253*, 235–249. [CrossRef]
6. Syed Annuar, S.N.; Kamaludin, N.F.; Awang, N.; Chan, K.M. Cellular Basis of Organotin(IV) Derivatives as Anticancer Metallo-drugs: A Review. *Front. Chem.* **2021**, *9*, 657599. [CrossRef]
7. Hazra, S.; Paul, A.; Sharma, G.; Koch, B.; da Silva, M.F.C.G.; Pombeiro, A.J.L. Sulfonated Schiff base Sn(IV) complexes as potential anticancer agents. *J. Inorg. Biochem.* **2016**, *162*, 83–95. [CrossRef]

8. Silva, A.; Luís, D.; Santos, S.; Silva, J.; Mendo, A.S.; Coito, L.; Silva, T.F.S.; Silva, M.F.C.G.d.; Martins, L.M.D.R.S.; Pombeiro, A.J.L.; et al. Biological characterization of the antiproliferative potential of Co(II) and Sn(IV) coordination compounds in human cancer cell lines: A comparative proteomic approach. *Drug Metabol. Drug Interact.* **2013**, *28*, 167–176. [[CrossRef](#)]
9. Milaeva, E.R.; Shpakovsky, D.B.; Gracheva, Y.A.; Antonenko, T.A.; Ksenofontova, T.D.; Nikitin, E.A.; Berseneva, D.A. Novel selective anticancer agents based on Sn and Au complexes. Mini-review. *Pure Appl. Chem.* **2020**, *92*, 1201–1216. [[CrossRef](#)]
10. Hong, M.; Chang, G.; Li, R.; Niu, M. Anti-proliferative activity and DNA/BSA interactions of five mono- or di-organotin(IV) compounds derived from 2-hydroxy-N'-[(2-hydroxy-3-methoxyphenyl)methylidene]-benzohydrazone. *New J. Chem.* **2016**, *40*, 7889–7900. [[CrossRef](#)]
11. Banti, C.N.; Hadjikakou, S.K.; Sismanoglu, T.; Hadjiliadis, N. Anti-proliferative and antitumor activity of organotin(IV) compounds. An overview of the last decade and future perspectives. *J. Inorg. Biochem.* **2019**, *194*, 114–152. [[CrossRef](#)]
12. Attanzio, A.; D'Agostino, S.; Busà, R.; Frazzitta, A.; Rubino, S.; Girasolo, M.A.; Sabatino, P.; Tesoriere, L. Cytotoxic Activity of Organotin(IV) Derivatives with Triazolopyrimidine Containing Exocyclic Oxygen Atoms. *Molecules* **2020**, *25*, 859. [[CrossRef](#)] [[PubMed](#)]
13. Amir, M.K.; Khan, S.Z.; Hayat, F.; Hassan, A.; Butler, I.S.; Zia-ur-Rehman. Anticancer activity, DNA-binding and DNA-denaturing aptitude of palladium(II) dithiocarbamates. *Inorg. Chim. Acta* **2016**, *451*, 31–40. [[CrossRef](#)]
14. Gielen, M. Review: Organotin compounds and their therapeutic potential: A report from the Organometallic Chemistry Department of the Free University of Brussels. *Appl. Organomet. Chem.* **2002**, *16*, 481–494. [[CrossRef](#)]
15. Tabassum, S.; Yadav, S.; Arjmand, F. Exploration of glycosylated-organotin(IV) complexes as anticancer drug candidates. *Inorg. Chim. Acta* **2014**, *423*, 38–45. [[CrossRef](#)]
16. Basu Baul, T.S.; Paul, A.; Pellerito, L.; Scopelliti, M.; Singh, P.; Verma, P.; de Vos, D. Triphenyltin(IV) 2-[(E)-2-(aryl)-1-diazenyl]benzoates as anticancer drugs: Synthesis, structural characterization, in vitro cytotoxicity and study of its influence towards the mechanistic role of some key enzymes. *Investig. New Drugs* **2010**, *28*, 587–599. [[CrossRef](#)]
17. Pruchnik, H.; Lis, T.; Latocha, M.; Zielińska, A.; Ułaszewski, S.; Pelińska, I.; Pruchnik, F.P. Butyltin(IV) 2-sulfobenzoates: Synthesis, structural characterization and their cytostatic and antibacterial activities. *J. Inorg. Biochem.* **2012**, *111*, 25–32. [[CrossRef](#)]
18. Saxena, A.K.; Huber, F. Organotin compounds and cancer chemotherapy. *Coord. Chem. Rev.* **1989**, *95*, 109–123. [[CrossRef](#)]
19. Kolyada, M.; Osipova, V.; Berberova, N.; Pimenov, Y.; Milaeva, E. Decline of Prooxidant Activity of Butyl and Phenyl Derivatives of Tin in the Presence of meso-Tetrakis(3,5-di-tert-butyl-4-hydroxyphenyl)porphyrin. *Macroheterocycles* **2017**, *10*, 57–61. [[CrossRef](#)]
20. Murumkar, P.R.; Ghuge, R.B. Chapter 9—Vicinal Diaryl Oxadiazoles, Oxazoles, and Isoxazoles. In *Vicinal Diaryl Substituted Heterocycles*; Elsevier: Amsterdam, The Netherlands, 2018; pp. 277–303.
21. Briguglio, I.; Piras, S.; Corona, P.; Gavini, E.; Nieddu, M.; Boatto, G.; Carta, A. Benzotriazole: An overview of its versatile biological behavior. *Eur. J. Med. Chem.* **2015**, *97*, 612–648. [[CrossRef](#)]
22. Hall, C.D.; Panda, S.S. The Benzotriazole Story. *Adv. Heterocycl. Chem.* **2016**, *119*, 1–23.
23. Loukopoulos, E.; Kostakis, G. Recent advances in the coordination chemistry of benzotriazole ligands. *Coord. Chem. Rev.* **2019**, *395*, 193–229. [[CrossRef](#)]
24. Stamou, C.; Lada, Z.G.; Paschalidou, S.; Chasapis, C.T.; Perlepes, S.P. Towards Construction of the “Periodic Table” of 1-methylbenzotriazole (review). *Inorganics* **2024**, *12*, 208. [[CrossRef](#)]
25. Sheldrick, G.M. *SADABS, Version 2.03*; Bruker Analytical X-ray Systems: Madison, WI, USA, 2000.
26. Sheldrick, G. SHELXT—Integrated space-group and crystal-structure determination. *Acta Cryst. A* **2015**, *71*, 3–8. [[CrossRef](#)]
27. Sheldrick, G. Crystal structure refinement with SHELXL. *Acta Cryst. C* **2015**, *71*, 3–8. [[CrossRef](#)] [[PubMed](#)]
28. Stamou, C.; Barouni, E.; Plakatouras, J.C.; Sigalas, M.M.; Raptopoulou, C.P.; Psycharis, V.; Bakalbassis, E.G.; Perlepes, S.P. The “Periodic Table” of 1-methylbenzotriazole: Zinc(II) Complexes. *Inorganics* **2023**, *11*, 356. [[CrossRef](#)]
29. Edgell, W.F.; Ward, C.H. The Raman and infrared spectra of the series (CH₃)_nSnCl_(4-n). *J. Mol. Spectrosc.* **1962**, *8*, 343–364. [[CrossRef](#)]
30. Dimitropoulos, A.; Stamou, C.; Sp, P.; Lada, Z.; Petsalakis, I.; Marinakis, S. A Study of 1-Methylbenzotriazole (MEBTA) Using Quantum Mechanical Calculations and Vibrational, Electronic, and Nuclear Magnetic Resonance Spectroscopies. *J. Eng. Sci. Technol. Rev.* **2023**, *16*, 77–84. [[CrossRef](#)]
31. Cardin, C.J.; Roy, A. Anticancer activity of organotin compounds. 2. Interaction of diorganotin dihalides with nucleic acid bases and nucleosides; the synthesis of adenine, adenosine and 9-methyladenine adducts. *Inorg. Chim. Acta* **1985**, *107*, 57–61. [[CrossRef](#)]
32. Alberte, B.; Sánchez González, A.; García, E.; Casas, J.S.; Sordo, J.; Castellano, E.E. Complexes of dimethyldihalotin(IV) with imidazole and pyrazole: The crystal structure of dibromobis(pyrazole)dimethyltin(IV). *J. Organomet. Chem.* **1988**, *338*, 187–193. [[CrossRef](#)]
33. Geary, W.J. The use of conductivity measurements in organic solvents for the characterization of coordination compounds. *Coord. Chem. Rev.* **1971**, *7*, 81–122. [[CrossRef](#)]
34. Ceballos-Torres, J.; del Hierro, I.; Prashar, S.; Fajardo, M.; Mijatović, S.; Maksimović-Ivanić, D.; Kaluđerović, G.N.; Gómez-Ruiz, S. Alkenyl-substituted titanocene dichloride complexes: Stability studies, binding and cytotoxicity. *J. Organomet. Chem.* **2014**, *769*, 46–57. [[CrossRef](#)]
35. Sharma, A.; Dhingra, N.; Singh, H.L.; Khaturia, S.; Bhardawaj, U. New Complexes of organotin(IV) and organosilicon(IV) with 2-[(3,4-dimethoxybenzylidene)amino]-benzenethiol: Synthesis, spectral, theoretical, antibacterial, docking studies. *J. Mol. Struct.* **2022**, *1261*, 132812. [[CrossRef](#)]

36. Shahzadi, S.; Ali, S. Structural Chemistry of Organotin(IV) Complexes. *J. Iran. Chem. Soc.* **2008**, *5*, 16–28. [[CrossRef](#)]
37. Mangani, S.; Piperigkou, Z.; Koletsis, N.; Ioannou, P.; Karamanos, N.K. Estrogen receptors and extracellular matrix: The critical interplay in cancer development and progression. *FEBS J.* 2024; *in press*. [[CrossRef](#)]

Disclaimer/Publisher's Note: The statements, opinions and data contained in all publications are solely those of the individual author(s) and contributor(s) and not of MDPI and/or the editor(s). MDPI and/or the editor(s) disclaim responsibility for any injury to people or property resulting from any ideas, methods, instructions or products referred to in the content.